Journal of Renewable Materials

Tech Science Press

https://doi.org/10.32604/jrm.2026.02026-0062

ARTICLE

Developing a Tannin-Furanic Foam with Excellent Thermal Insulation and Robust Flame Retardancy via the Synergistic Effect of Phytic Acid

Wenhe Bi[1], Yang Yang[1], Jiamin Wu[1], Jianji Chu[2], Jun Zhang[1], Guanben Du[1], Hisham Essawy[3], Bertrand Charrier[4], Antonio Pizzi[5], Xinyi Chen[1,*], Mingzhi Zhu[6,*] and Xiaojian Zhou[1,*]

[1]Yunnan Provincial Key Laboratory of Wood and Bamboo Biomass Materials, Southwest Forestry University, Kunming, China
[2]Yunnan Xinze Xing Wood-Based Panel Co., Ltd., Kunming, China
[3]Department of Polymers and Pigments, National Research Centre, Cairo, Egypt
[4]CNRS/Univ Pau & Pays Adour, Institut des Sciences Analytiques et de Physico-Chimie pour l'Environnement et les Matériaux-Xylomat, UMR5254, Mont-de-Marsan, France
[5]LERMAB, University of Lorraine, 27 rue Philippe Seguin, Epinal, France
[6]National Research Center of Engineering and Technology for Utilization of Botanical Functional Ingredients, Key Laboratory of Tea Science of Ministry of Education, College of Horticulture, Hunan Agricultural University, Changsha, China

*Corresponding Authors: Xinyi Chen. Email: chen_xinyi_csuft@126.com; Mingzhi Zhu. Email: mzzhucn@hotmail.com; Xiaojian Zhou. Email: xiaojianzhou@swfu.edu.cn

Received: 28 April 2026; Accepted: 08 June 2026; Published: 29 June 2026

ABSTRACT: It is *p*-toluenesulfonic acid (*p*-TSA) that is commonly used as a catalyst in conventional tannin-furanic foams. However, it does not participate in the crosslinking network and tends to leach out from the foam during use, resulting in a strongly acidic material that may corrode contacting substrates and accelerate material aging. To address this issue, herein, tannin and furfuryl alcohol were used as raw materials, and bio-derived phytic acid (PA) was employed to completely replace *p*-TSA for the preparation of tannin-furanic foams. The multi-phosphate groups of PA form a stable crosslinked network with tannin, thereby anchoring the catalyst in the foam matrix. Inductively coupled plasma (ICP) and energy-dispersive X-ray spectroscopy (EDS) analyses revealed that the leaching ratio of *p*-TSA from the foam was as high as approximately 92%, whereas the leaching ratio of PA reached about 78%, demonstrating the superior loading stability of PA. The as-prepared tannin-furanic foam exhibited a compressive strength of 0.137 MPa, which is approximately 49% higher than that of the foam catalyzed by *p*-TSA. Ignition tests confirmed that the prepared tannin-furanic foam possessed excellent flame retardancy, with a limiting oxygen index (LOI) exceeding 70%, much higher than that of conventional foam (ca. 38%). This study provides an effective route for the development of an eco-friendly tannin-furanic foam material with excellent flame retardancy.

KEYWORDS: Tannin-furanic foams; phytic acid (PA); acid leach out; flame retardancy

1 Introduction

Since the first report [1], tannin-furanic foams have received considerable interest for their excellent properties, such as lightweight, flame retardancy, and thermal insulation. The classical formulation contains bio-derived tannin and furfuryl alcohol, formaldehyde (crosslinker), *p*-toluenesulfonic acid (*p*-TSA, acid catalyst), and diethyl ether (DE, foaming agent). Notably, this foam can be prepared by self-foaming at room temperature without requiring sophisticated equipment and process. The obtained foam products exhibit low density (around 50 kg/m^3), low thermal conductivity (down to 0.045 W/(m·K)), and a limiting oxygen index (LOI) close to 30, which are comparable to those of commercial foams such as polyurethane (PU)

foams [2,3], polystyrene foams (PS) [4,5], and phenol-formaldehyde foams [6] in some performance aspects. Consequently, tannin-furanic foams can be considered as promising alternatives to petroleum-based non-renewable foams in construction and packaging fields [7,8].

Nevertheless, the traditional tannin-furanic foam still has some flaws, such as formaldehyde and DE utilization, and insufficient mechanical strength. Subsequent updating studies were carried out. Typically, some alternative crosslinkers such as glyoxal, glutaraldehyde [9], and soybean protein [10] have been used to reduce or replace formaldehyde for formulation updating. Novel foaming approaches have been successfully proposed, i.e., mechanical stirring and steam-driven foaming, for addressing the environmental and health concerns caused by traditional physical/chemical blowing agents (e.g., azodicarbonamide (AC) [11] and DE [10]). Moreover, strategies such as incorporating reinforcement materials (e.g., lignin [12] and polymeric methylene diphenyl diisocyanate (p-MDI) [13], or constructing sandwich [14]/double-layer structures [15] have been employed to overcome the inherent brittleness and insufficient mechanical strength.

Progress has been made in improving the comprehensive performance and environmental protection performance of the foam. However, a critical issue remains. The preparation of tannin-furanic foams requires *p*-TSA to initiate the poly-condensation of furfuryl alcohol and ensure effective cross-linking. Since the *p*-TSA does not participate in the final three-dimensional network build, it can gradually leach out from the foam during practical application, causing the foam itself to be strongly acidic and potentially corroding contacting materials or accelerating material aging [16]. Therefore, seeking an alternative acid that can both effectively catalyze the cross-linking and be firmly anchored in the foam matrix is of great significance for improving the practicality and environmental friendliness of tannin-furanic foams.

Phytic acid (PA) is an organic acid that is biologically compatible, eco-friendly, non-hazardous, and easily accessible. It offers broad application in fields such as food, pharmaceuticals, metal processing, household products, paints and coatings, textiles, plastics processing, and the polymer industry [17]. Crucially, the acidic environment it provides fully meets the basic requirements necessary for catalyzing the cross-linking reaction of tannin-furanic resin [18]. Therefore, considering the environmental attributes and basic molding requirements of tannin-furanic foam, PA can meet the requirements of replacing *p*-TSA. In addition, it contains six phosphate groups, which can form a tight network with tannin through chelation or covalent crosslinking, thereby being firmly fixed in the foam and reducing migration [19], which was proved in our previous work. Because it participates in forming a cross-linked structure, it can enhance the overall mechanical strength of the foam material. Interestingly, PA is also a commonly used flame retardant and is widely applied in the development of biomass materials. When it is introduced into the composition of tannin-furanic foam, the flame retardancy of the foam can effectively be further improved, relying on the inherent flame-retardant properties of the raw materials [19,20]. These unique properties have enabled PA to demonstrate significant advantages and potential in the development of tannin-furanic foam materials, effectively addressing the environmental and health issues posed by *p*-TSA.

Herein, PA is considered as an acid catalyst in tannin-furanic foam formulation for completely replacing *p*-TSA, and mechanical stirring was adopted to prepare tannin-furanic-PA foam assisted by sodium bicarbonate as the blowing agent. The loading stability of *p*-TSA and PA in the foams was evaluated. Furthermore, the crosslinking mechanism was proposed as further evidence to support the effectiveness of the PA replacement strategy. Then, the resultant foam products were systematically analyzed and investigated in terms of morphology, mechanical properties, thermal stability, thermal conductivity, and flame retardancy. Compared with conventional tannin-furanic foam catalyzed by *p*-TSA, the tannin-furanic-PA foam exhibits better comprehensive performance. This approach provides an environmentally friendly strategy for modifying tannin-furanic foams, offering a sustainable pathway to improve their performance without relying on petrochemical-derived additives.

2 Materials and Methods

2.1 Materials

Commercial mimosa tannin extract (from the Acacia tree, TA) was supplied by TANAC S/A (R. Torbjorn Weibul, Brazil). Shanghai Macklin Biochemical Technology Co, Ltd. provided furfuryl alcohol (FA, AR, 98%), formaldehyde (F, 37%), and phytic acid (PA, 70%). Sinopharm Chemical Reagent Co. Ltd. supplied Tween-80 (CP), sodium hydrogen carbonate ($NaHCO_3$), and *p*-toluenesulfonic acid (*p*-TSA, AR), deionized water (DW) was produced in the laboratory. Unless otherwise stated, all reagents were used without additional purification.

2.2 Preparation of Tannin-Furanic Foams

A 65% aqueous solution of *p*-TSA was prepared for standby.

Two types of tannin-furanic foam were involved in this work, that was catalyzed by *p*-TSA and PA, respectively (Scheme 1). The traditional tannin-furanic foam as a control group was obtained as follows: TA and FA were placed in a plastic beaker according to the formulation listed in Table 1 then mixed well. Afterwards, Tween-80, $NaHCO_3$, distilled water, and formaldehyde solution were added in turn and stirred well using a whisk. *p*-TSA was introduced into the mixture and rapidly stirred for 20 s to yield a liquid foam. The liquid foam was allowed to stand at ambient temperature for an additional 2 h to facilitate post-foaming, subsequently transferred to an oven at 80°C, and cured for a further 24 h. The control group was labelled as TFF.

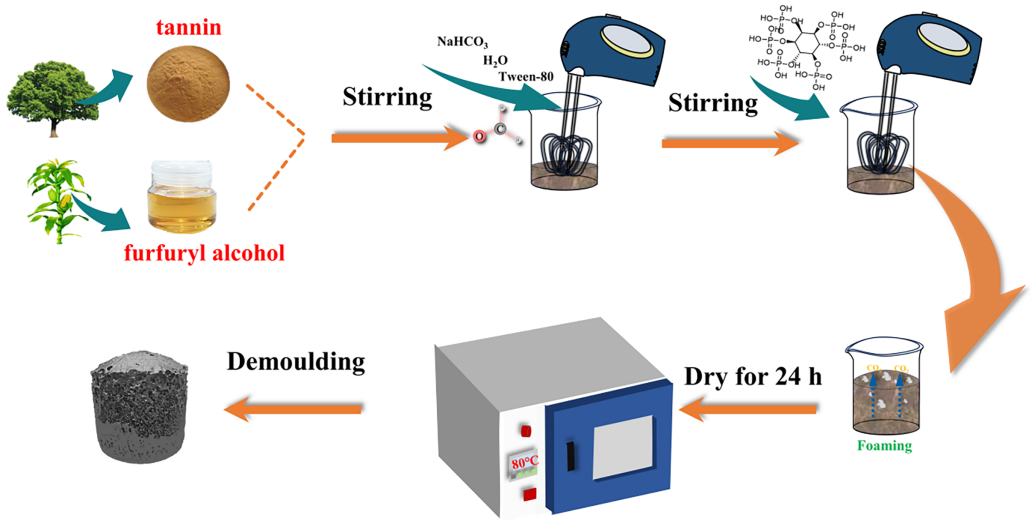

Scheme 1: Preparation steps of the foams.

Table 1: The formulations of tannin-furanic resin precursors.

Samples	TA/g	FA/g	DW/g	Tween-80/g	F/g	*p*-TSA/g	PA/g	$NaHCO_3$/g
TFF	60	30	5	1.5	15	20	–	3
TPF25	60	30	5	1.5	15	–	25	3
TPF30	60	30	5	1.5	15	–	30	3
TPF35	60	30	5	1.5	15	–	35	3

The target tannin-furanic-PA foam was synthesized with reference to the preparation protocol of TFF, wherein *p*-TSA was substituted with PA (Table 1). The as-obtained foams were named TPF25, TPF30, and TPF35, respectively, according to the added PA dosage.

Before final characterization, the foams were kept under ambient conditions (12°C–20°C, 40%–60% relative humidity (RH)) for a minimum of 2 days.

2.3 Characterizations

2.3.1 Apparent Density Measurements

In accordance with the national standard ASTM D1622-03 standard, the specimens were prepared into a size of 50 mm^3 × 50 mm^3 × 50 mm^3, and the foam's apparent density (ρ) was calculated by measuring the mass and volume of each specimen. The following formula was applied:

$$\rho = \frac{m}{v}$$

where m denotes the specimen mass in kg, v denotes its volume in m^3, ρ represents the apparent density of the sample (kg/m^3), and the average apparent density is obtained through 5 repeated measurements.

2.3.2 Mechanical Properties

According to the GB/T 8813-2020 standard, the foam was prepared into 30 mm^3 × 30 mm^3 × 30 mm^3 specimens with smooth and flat surfaces. A universal mechanical testing machine (AG-50KN, Shimadzu, Japan) was employed to measure the compressive strength at a fixed loading rate of 2 mm/min until specimen failure. The accompanying software of the instrument recorded the stress-strain curve. The compressive strength was then derived using the equation below:

$$Compression\ stress = \frac{F_{max}}{S}$$

here, F_{max} denotes the peak force (N) applied before reaching 10% strain, and S is the specimen's load-bearing area (mm^2). The final strength value was averaged from five repeated measurements (MPa).

2.3.3 The Pulverization Ratio

Following the GB/T 12812-2006Z standard, a foam specimen of 50 mm^3 × 50 mm^3 × 50 mm^3 was cut. Its initial mass, denoted as M_0 (kg), was measured. The specimen was then laid horizontally onto a 250-mm-long piece of 400-mesh sandpaper, with a 200 g weight placed on it. A tensile test was repeated 30 times under a constant loading speed of 10 mm/s. After the test, the remaining mass of the foam, M_1 (kg), was recorded. The pulverization ratio was then derived using the formula below:

$$Pulverization\ ratio = \frac{M_0 - M_1}{M_0} \times 100\%$$

The pulverization ratio (%) was obtained from 5 repeated measurements.

2.3.4 The Thermal Conductivity

Foam samples were cut into cylinders (radius: 50 mm, thickness: 10 mm), and the thermal conductivity was measured using a YBF-2 apparatus from Dahua Ltd., Hangzhou. Subsequently, the following formula was used for calculation:

$$\lambda = -mc\frac{2h_p + R_P}{2h_p + 2R_P} * \frac{1}{\pi R^2} * \frac{h}{T_1 - T_2} * \frac{dT}{d\tau} \Big/ T = T_2$$

In this formula, λ denotes the thermal conductivity in W/(m·K). The symbols m and c refer to the mass and specific heat capacity, respectively, of the copper plate located at the bottom of the instrument. The sample's cutting surface has a radius R of 50 mm and a thickness h of 10 mm, while the bottom copper plate possesses a radius R_P of 50 mm and a thickness h_p of 10 mm. The temperature difference between the upper and lower surfaces of the copper plate is expressed as $T_1 - T_2$.

2.3.5 Acid Leaching Test

To evaluate the leaching behavior of the catalysts in the foam matrix, an acid leaching test was conducted. Foam samples were cut into small pieces. then immersed in distilled water and left to stand at room temperature for 24 h. The initial pH of distilled water was recorded before immersion, and the final pH was measured after the soaking process using a calibrated pH meter. After leaching, the foam samples were removed, rinsed with distilled water, and then oven-heated at 60°C to a constant weight for further analysis.

2.3.6 ICP Analysis

The elemental content of sulfur (S) and phosphorus (P) in the foam samples before and after the leaching test was determined by inductively coupled plasma optical emission spectroscopy (ICP-OES) using an Agilent 725-ES instrument from the USA.

2.3.7 Microscopic Morphology

The foam was cut into cubes of 10 mm^3 × 10 mm^3 × 10 mm^3 and observed with a scanning electron microscope (SEM), model ZEISS Gemini SEM 300, manufactured in Germany, using an acceleration voltage of 15 kV. A Leica EM ACE600 high vacuum sputtering coater was used to sputter a thin gold film on the surface of each sample to improve electrical conductivity.

2.3.8 Thermal Stability Evaluation

Using a Netzsch STA 2500 thermogravimetric system (TGA, Germany), the thermal stability of the foams was evaluated under a flowing nitrogen atmosphere, on samples weighing 5–8 mg, which were heated from ambient temperature to 790°C at a rate of 10°C/min for each cycle.

2.3.9 The Flame Retardancy Evaluation

The flame retardancy was tested according to GB/T2406.2-2009 using Tech-GBT2406-1 oxygen index tester (Testech Co., Ltd., China). Foam samples with a size of 80 mm^3 × 10 mm^3 × 4 mm^3 were prepared by the top ignition method.

Foam samples of 30 mm^3 × 30 mm^3 × 30 mm^3 were selected for the ignition test. Without any shielding, the foam was placed on the jet flame produced by the butane flamethrower. A high-resolution digital camera was used to record the entire ignition experiment. Using a cone calorimeter (CC, FTT, UK) while following ISO 5660, the combustion behavior of the control and test samples was measured on specimens of 100 mm^3 × 100 mm^3 × 50 mm^3 under a heat flux of 35 kW/m^2.

3 Results and Discussion

3.1 Assessment of Acid Leaching Behavior and Catalyst Stability

It should be noted that sample selection was based on the overall foam performance. When the S and P elemental ratios were normalized by molar mass, using either *p*-TSA or PA as the benchmark failed to produce a foam with satisfactory performance.

The TFF and TPF30 were selected to verify the stability of *p*-TSA and PA in the foam matrix. The pH of the leachate was recorded prior to and following immersion of the foam, and the corresponding results are presented in Table 2. The acid leaching was observed in both TFF and TPF30, manifested by marked reductions in pH. Specifically, the pH decreased from 7.34 to 3.85 for TFF and from 7.36 to 4.24 for TPF30. ICP analysis indicated a 92.40% reduction in S content (from *p*-TSA) for TFF after immersion, compared to a 78.29% decrease in P content (from PA) for TPF30. EDS-mapping results (Fig. 1) provided further evidence for this finding. Following leaching, the S signal in TFF-2 became negligible, while a distinct P signal remained.

Table 2: The pH and concentration of foam element precipitation.

Samples	Initial pH	Final pH	Initial Load of S/P in Foam (%)	Final load of S/P in Foam (%)	Proportion of S/P Elemental Precipitation (%)
TFF	7.34	3.85	2.38	0.18	92.40
TPF30	7.36	4.24	4.62	1.01	78.29

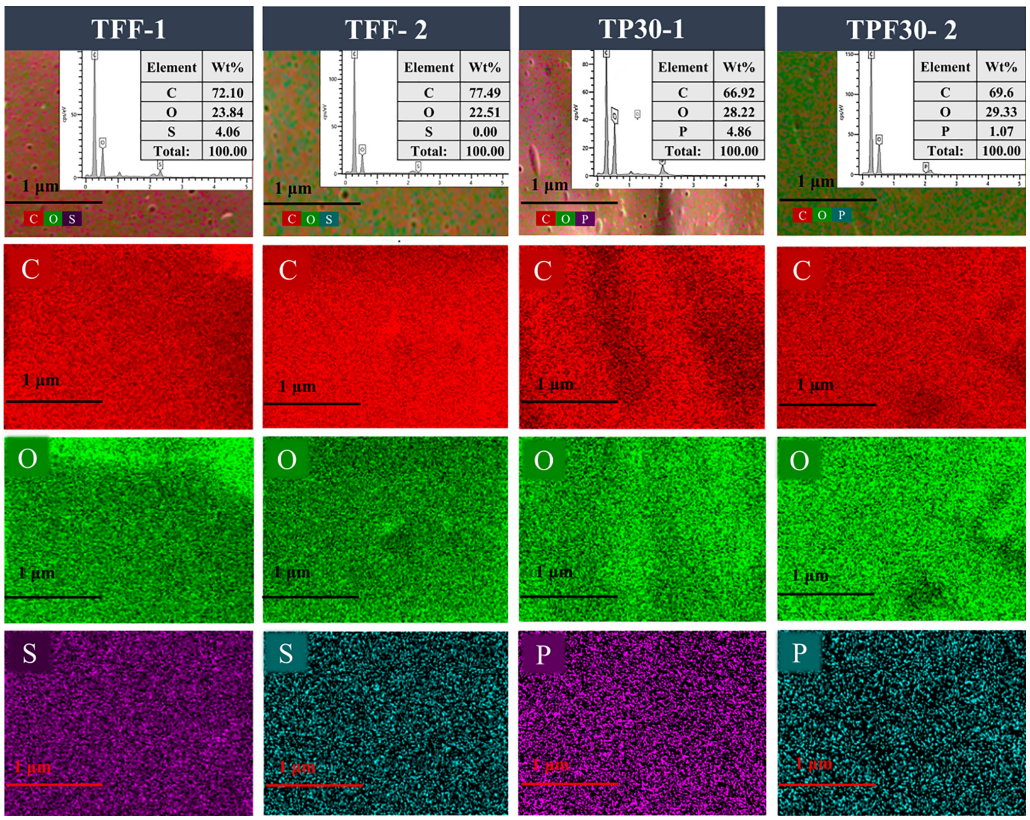

Figure 1: EDS spectrum and the EDS elemental mapping images.

Detectable in TPF30-2. The content of phosphorus decreased from 4.86% to 1.07%, corresponding to a reduction of approximately 78%, which aligns well with the ICP results.

The abovementioned phenomenon can state the fact that a certain amount of PA was fixed in the foam TPF30. This is because the unique phosphate groups of PA can undergo condensation reactions with the phenolic hydroxyl groups of tannin and furfuryl alcohol during the curing process, forming stable covalent bonds. This cross-linking mechanism was reported in our previous work. Nevertheless, the degree of covalent crosslinking remains constrained, given that the foam is cured at relatively mild temperatures (80°C for 24 h).

3.2 Proposed Cross-Linking Mechanism

The chemical structures of the raw materials and resulting foams were further characterized using Fourier transform infrared (FT-IR) spectroscopy. Fig. 2a shows the FT-IR spectra of TA, PA, FA, and tannin-furanic foams (TFF and series TPF). The FT-IR spectrum of TA showed characteristic O-H stretching and bending vibrations at 3382 and 1347 cm^{-1}, respectively. The C-O stretching of the ether bridge appeared at 1111 and 1029 cm^{-1}, while the benzene ring skeleton gave rise to peaks at 1611, 1508, and 1452 cm^{-1} [21,22]. In the PA spectrum, there are absorption bands at 3410 and 1640 cm^{-1}, corresponding to the antisymmetric stretching vibration of O-H in aqueous solution and the bending vibration of water molecules, respectively [23,24]. The peak at 2850 cm^{-1} is characteristic of P-OH stretching. The peak at 1126 cm^{-1} arises from the P=O stretching vibration, while the peaks at 1052 and 1012 cm^{-1} are attributed to the P-O stretching vibrations in the $(PO3)^{2-}$ and P-O-C structures, respectively [24,25].

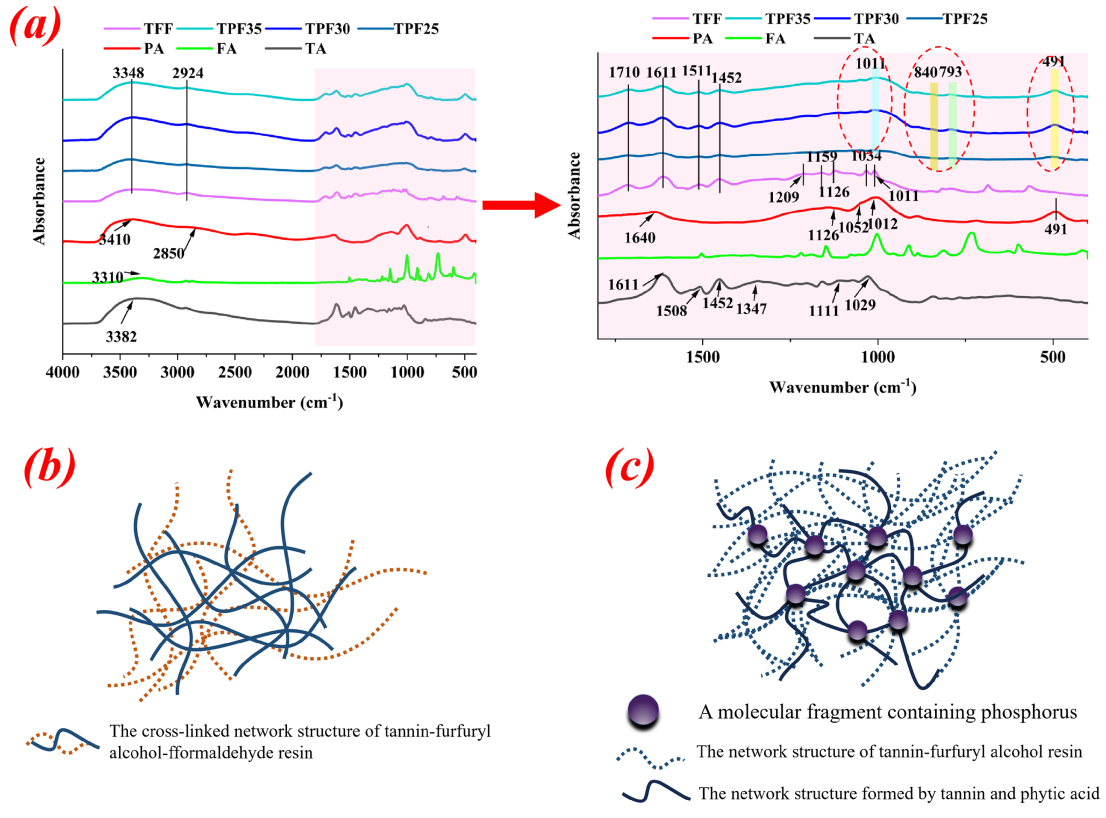

Figure 2: FT-IR spectra of TA, PA, FA, and tannin-furanic foam (TFF and series TPF) (**a**); The suggested cross-linked network structure of conventional tannin-furanic foam (**b**); The suggested cross-linked network structure of tannin-furanic-PA foam (**c**).

The FT-IR spectra of all prepared foam samples in Fig. 2a were found to be similar. A broad band corresponding to O-H stretching vibrations was observed in the range of 3500–3100 cm^{-1} (centered at 3348 cm^{-1}) while absorption peaks from the symmetric and asymmetric stretching vibrations of CH_2/CH_3 groups appeared at 2924 cm^{-1} (Region II) [26]. Furthermore, the peak at 1710 cm^{-1} is attributed to C=O stretching vibration, while the sharp peaks at 1611 and 1511 cm^{-1} correspond to benzene skeleton vibrations and the phenol hydroxyl groups on the benzene ring, respectively [27]. The strong absorption peak at 1452 cm^{-1}, suggests the formation of methylene (-CH_2–) groups, possibly via condensation between furfuryl alcohol and tannin flavonoids under catalysis by either PA or *p*-TSA [28,29].

For the TFF foam, C-O and C-C stretching vibrations were observed at 1209, 1159, 1126, and 1034 cm^{-1}, confirming partial self-polycondensation of furfuryl alcohol. In the tannin-furanic-PA (TPF) foams [16], the characteristic peak of PA at 491 cm^{-1} was retained, providing a distinctive marker for these foams. Moreover, the expansion of P-O-C bonds in PA at 1011, 840, and 793 cm^{-1} contributed to the increased peak area at ~1010 cm^{-1} in the TPF foams, further demonstrating that PA was successfully incorporated into the foam matrix [30].

As evidenced by FT-IR signatures of P-O-C bonds and the retained P element distribution in EDS-mapping (Fig. 1), PA became possibly covalently anchored within the tannin-furanic matrix. This chemical fixation results in markedly lower leaching compared to the physically entrapped *p*-TSA. The proposed cross-linking mechanism of TFF and TPF is shown in Fig. 2b,c. The cross-linking effect involving PA also enhances the mechanical properties of TPF foam.

3.3 Physical and Mechanical Properties

Table 3 summarizes the measured physical-mechanical parameters (apparent density, pulverization ratio, and compressive strength) for the TFF and TPF foams. The density of TFF was 93.07 kg/m^3. The densities of TPF30 and TPF35 were 101.31 and 96.56 kg/m^3, respectively, comparable to those of conventional tannin-furanic-formaldehyde foams reported in the literature [31,32], demonstrating that the PA-based formulation achieved comparable lightweight characteristics without relying on *p*-TSA. However, TPF25 had a density of 162.38 kg/m^3, which significantly exceeds the normal range of the density of tannin-furanic foams. The reason for this outcome is that the acidic environment provided by PA is insufficient to generate the heat required for complete foaming of the precursors. The height of the TPF25 foam in Fig. 3a can confirm this view. As evident from the SEM micrographs (Fig. 3b), TPF25 possesses a non-uniform and thickened cell wall structure relative to TFF, which correlates with its increased density. In contrast, as the PA content increases, the foaming height of TPF rises (Fig. 3a), and the SEM images (Fig. 3b) reveal a more developed porous structure, leading to a progressive decrease in density.

Table 3: Physical properties data of the foams.

Samples	Apparent Density (kg/m^3)	Pulverization Ratio (%)	Compression Strength (MPa)
TFF	93.07 (±3.77)	7.72 (±0.91)	0.092 (±0.014)
TPF25	162.38 (±5.79)	4.77 (±0.75)	0.362 (±0.021)
TPF30	101.31 (±3.48)	6.33 (±0.82)	0.137 (±0.019)
TPF35	96.56 (±4.83)	7.52 (±0.88)	0.124 (±0.017)

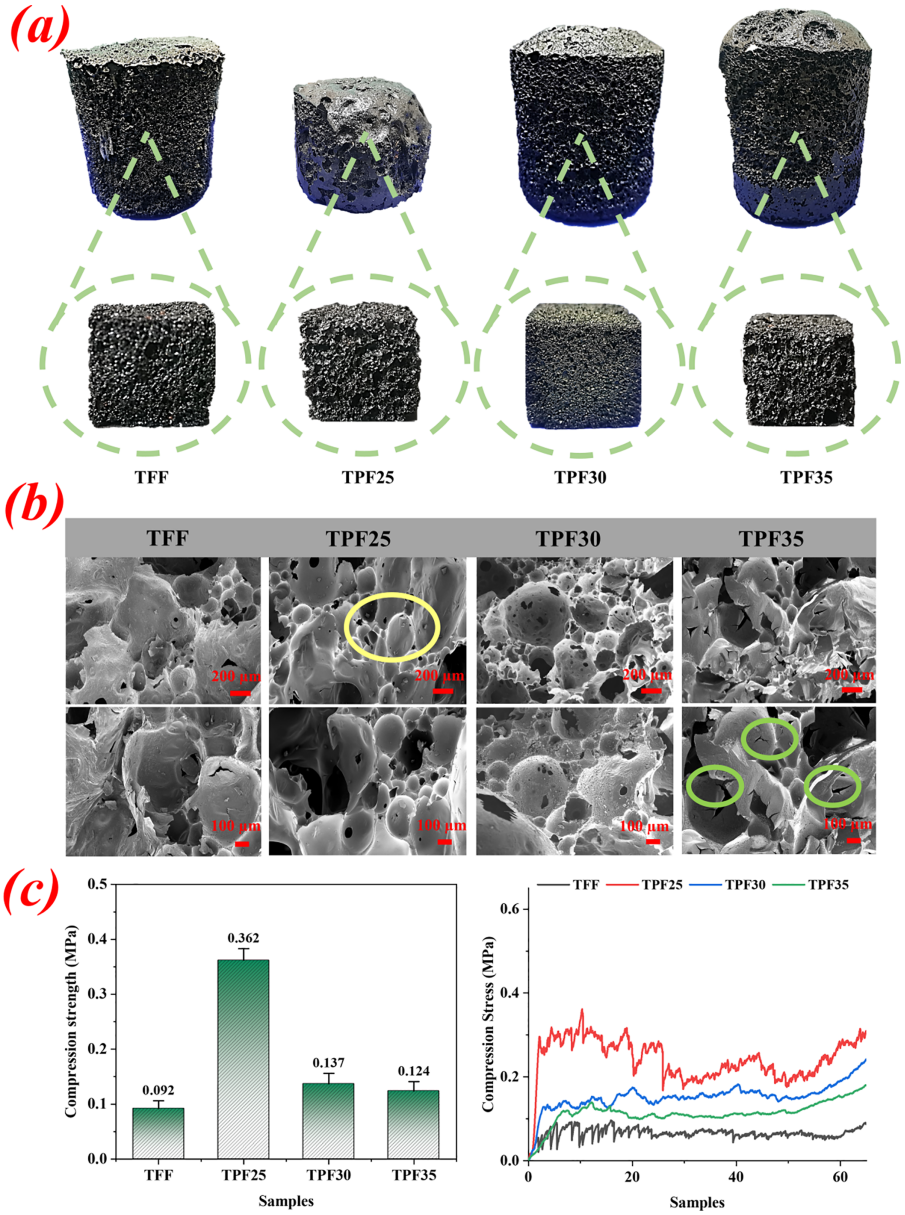

Figure 3: Foam products (**a**), SEM images of the foams (**b**) and stress-strain relations of the foams (**c**).

As shown in Table 3, the TFF foam exhibited the highest pulverization ratio of 7.72%. TPF35 showed a comparable value of 7.52%, indicating a negligible improvement over the control. This is attributed to the inherently low densities of highly expanded tannin-furanic foams (Fig. 3a), which compromise mechanical robustness [15]. In contrast, TPF25 and TPF30 achieved significantly lower pulverization ratios of 4.77% and 6.33%, respectively, corresponding to 38% and 18% reductions relative to TFF. This enhancement is ascribed to their denser, more crosslinked network structures-particularly for TPF25, where the uneven yet thickened cell walls (Fig. 3b) contribute to the improved structural integrity despite the overall low density of the foam system. Thus, the lower pulverization ratio of TPF indicates that these foams can better maintain their original shape and reduce particle detachment, which is of great significance for long-term handling, dust control, and dimensional stability of TPF materials during service.

Fig. 3c shows the corresponding stress-strain relations and compression strength data of TFF and a series of TPF foams under compressive loading. The observed deformation in the curves is consistent with the general trend for polymeric foams under compression [33,34]. The compression strength of the TPF series is higher than that of TFF, which is probably related to the increased foam density. By combining Table 2 and Fig. 3c, it can be observed that in this work, the density and compressive strength of the foam material are positively correlated. TPF25 achieved the highest compressive strength. There is no doubt that it is inseparable from its relatively high density. In contrast, the compressive strength of TPF30 is 0.137 MPa. By comparing TFF and TPF25, it can be observed that under similar density conditions (with the density increasing by only about 4%), the compressive strength of TPF25 is nearly 34% higher than that of TFF. This indicates that the enhancement in the strength of the TPF foam material is not solely dependent on the increase in its density. Indirectly, it was demonstrated that due to the substitution of PA, it partially contributed to the construction of the foam skeleton, thereby enhancing the overall strength of the foam. From Fig. 3, it can be seen that the overall structure (apparent properties in Fig. 3a and microstructure in Fig. 3b) of the TPF35 foam exhibits significant defects, with obvious collapse of the cell structure and cracks. Additionally, the cells are in an extremely uneven state. This is extremely unfavorable for maintaining a good compressive strength.

3.4 Characterization of Thermal Stability and Thermal Conductivity

The thermal conductivity of TFF and the series of TPF foams are shown in Fig. 4a. The thermal conductivity of the as-prepared TPF foams ranges from 0.0404 to 0.0460 W/(m·K), which is lower than that of the control TFF foam (0.0518 W/(m·K)) due to the larger cell wall of TFF, as shown in Fig. 3b. For the series of TPF foams, their thermal conductivity ranges from 0.0404 to 0.0460 W/(m·K), which is similar to the thermal conductivity of the previously reported tannin-furanic foam materials. Upon comparison, it was found that the TPF30 foam has the lowest thermal conductivity (0.0404 W/(m·K)). By combining Table 3 and Fig. 3b, it can be observed that TPF30 has an appropriate density and a relatively uniform foam cell structure. For TPF25 (0.0436 W/(m·K)), the rise in thermal conductivity is primarily due to the uneven pore structure and high relative density. Although the relative density of TPF35 is relatively low, its uneven pore structure leads to a relatively increased thermal conductivity. TPF35 shows numerous cracks on the cell walls, a looser overall structure, and in some regions a stacked rather than a well-defined closed-cell configuration. Such structural defects impair the thermal insulation capability of the foam, causing its thermal conductivity to increase compared to TPF30. It is reported that the foam morphology significantly affects the thermal conductivity of polymer foams [15]. Nevertheless, the overall thermal conductivity of the series of TPF foam still meets the application requirements.

The thermal stability of TFF and TPF foams was investigated using thermogravimetric analysis (TGA) under a nitrogen atmosphere. The results are shown in Fig. 4b,c, and their thermal parameters are summarized in Table 4. It can be found that the thermal decomposition trends of TFF and TPF are not the same. The first weight-loss of all foams appears at 25°C–100°C, which is attributed to adsorbed moisture evaporation [35–37]. By comparing the derivative thermogravimetry (DTG) curves of TPF and TFF, it can be realized that the weight loss of TPF at this stage is significantly higher than that of TFF, which may be due to the strong hygroscopic nature of PA. The second weight loss of the foams occurred between 100°C–250°C due to the polymer chains beginning to break into small molecules [33]. Compared with TFF, all TPF samples showed a lower onset temperature of weight-loss at this stage (195.7°C for TPF25, 195.6°C for TPF30, and 189.2°C for TPF35), and the peak temperature of weight loss (T_{max}) shifted to lower values with increasing PA content. This phenomenon can be attributed to the acidic species released from the phosphate groups of PA upon heating, which catalyze early cleavage of some chemical bonds in the foam structure, thereby

accelerating the initial degradation [38]. The third prominent weight-loss stage occurred between 250°C–350°C because of the C-C bond breaking in the polymer and the decomposition of the pyrolysis products. In addition, the thermal decomposition temperature of condensed tannins has been reported to be about 300°C, so this may be one of the causes of weightlessness at this stage [39]. Notably, with increasing PA content, the T_{max} of this stage slightly decreased from 301.4°C (TPF25) to 299.0°C (TPF30) and 297.3°C (TPF35). This indicates that although a higher concentration of PA promotes early degradation, it does not significantly alter the thermal cleavage mechanism of the main chain; instead, it promotes the preformation of char to some extent through its dehydration effect. For the control group and the experimental group at the last weight loss peak above 400°C, the break of the polymer chains can trigger the generation and liberation of a number of carbonaceous species possessing low molecular weights that coat the polymer surface, thereby forming an air-insulating layer on the polymer surface and enhancing the foam's thermal stability. For example, the aromatic skeleton of tannin has good thermal stability, but thermal decomposition occurs when the temperature is higher than 450°C [40]. TFF exhibits an obvious weight-loss peak at this stage (T_{max} = 476.3°C) with a weight loss rate as high as about 30%, corresponding to further pyrolysis of the carbon-rich aromatic structure and the release of volatile small molecules. In contrast, the weight loss peaks of all TPF samples above 400°C are greatly weakened or even disappear, and the char residue was significantly increased (53.67% for TPF25, 51.74% for TPF30, and 53.02% for TPF35, all higher than the 49.09% of TFF). This trend indicates that the addition of PA significantly facilitates the conversion of the foam matrix into a more stable and highly aromatic char layer at high temperatures. Particularly, when the PA content increases from 25 to 35 g, the char residue fluctuates slightly but remains at a high level, indicating that even at a lower PA content (25 g), its catalytic char-forming effect is already substantial; a further increase in PA content does not lead to a significant improvement in the char residue.

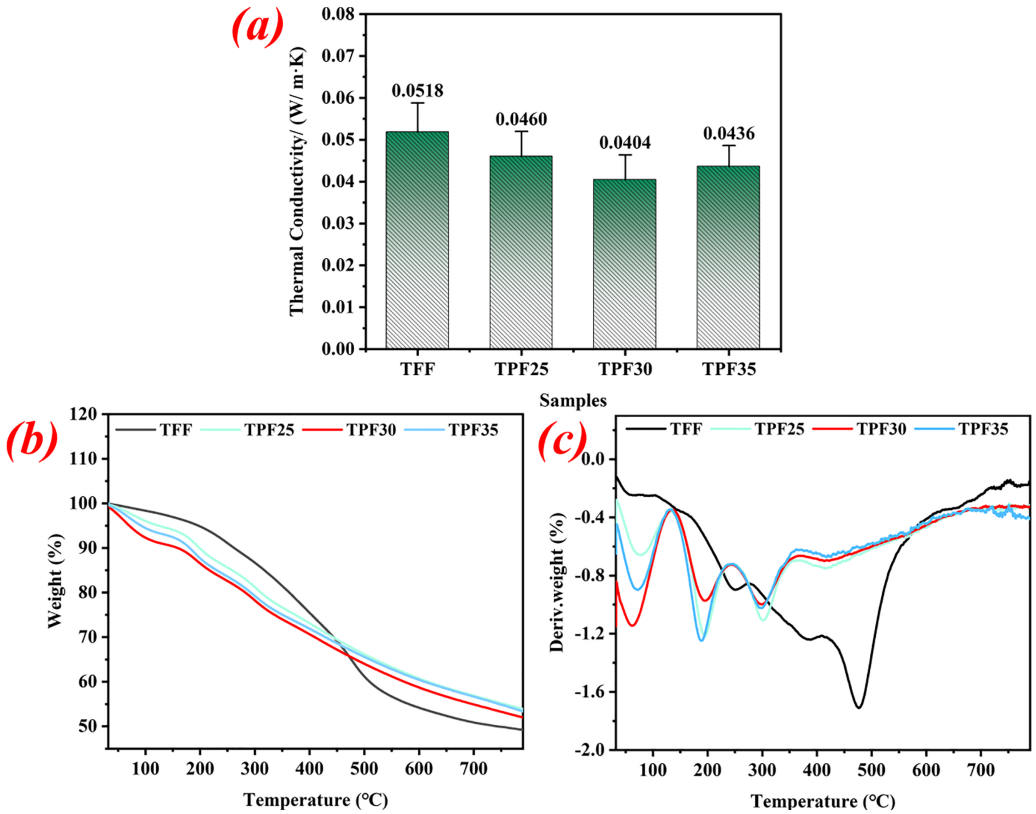

Figure 4: Thermal conductivity (**a**), TGA (**b**), and DTG (**c**) traces of the TFF and TPF foams series.

Table 4: TG data of TFF and a series of TPF foams.

Samples	T_{max} (°C)				Residual Mass at 790°C (%)
	Step I	Step II	Step III	Step IV	
TFF	55.30	250.06	382.8	476.3	49.09
TPF25	79.2	195.7	301.4	416.8	53.67
TPF30	81.7	195.6	299.0	419.2	51.74
TPF35	71.6	189.2	297.3	416.5	53.02

3.5 Evaluation of Flame-Retardant Performance

Ignition tests, limiting oxygen index (LOI) measurements, and cone calorimeter experiments were conducted to assess the flame retardancy of TPF. The outcomes are presented in Fig. 5. As presented in Fig. 5a, after continuous ignition for 180 s, neither TFF nor TPF exhibited any combustion behavior. However, in comparison, a carbon layer formed on the surface of TFF with some combustion defects, while TPF immediately lost its red glow after the flame was removed, showing no self-ignition behavior and no release of combustion smoke, indicating that TPF possesses superior self-extinguishing ability and good flame retardancy. To more intuitively demonstrate the advantages of TPF in flame retardancy, Fig. 5b displays the LOI data of TFF and TPF foams. TFF has an LOI value of 38.1%, indicating its good flame retardancy foundation, while TPF modified by PA exhibits LOI values above 70% (TPF25: 75.1%, TPF30: 73.8%, TPF35: 77.6%), demonstrating exceptionally excellent flame retardancy. The LOI value of TPF was compared with that of the traditional tannin-furanic acid foam catalyzed by *p*-TSA (Fig. 5c). The LOI values of conventional tannin-furanic foams are all under 50%, while the TPF developed in this study exhibits a markedly higher LOI [10,15,33,40–42]. Therefore, TPF has great advantages in flame retardancy.

Following the previous observations, cone calorimetry was used to characterize the flame retardancy features and mechanisms of TFF and TPF30. As seen in Fig. 5c,d and Table 5. The peak heat release rate (pHRR) of TFF is 67.81 kW/m^2, while that of TPF30 is only 24.09 kW/m^2, which is lower than most reported refractory materials [43,44]. Furthermore, TPF30 exhibits a total heat release (THR) of just 28.25 MJ/m^2, which is only 50% of that of TFF (56.72 MJ/m^2). These characteristics bring advantages to TPF30 in fire scenarios. Moreover, in fire scenarios, inhalation of toxic or harmful gases is often the greatest danger. Although the total smoke release (TSR) of TPF30 is 0.37 m^2, higher than that of TFF (0.18 m^2), the peak smoke production rate (pSPR) of TPF30 is far lower than that of TFF, providing a higher possibility for escape in fire scenarios. Fig. 5f shows the sample condition after cone calorimetry testing. After combustion, TPF30 exhibited more cracks than TFF, possibly due to the mismatch in thermal expansion behavior between the carbon layer and the foam matrix [45,46]. Notably, the residues of TPF30 after combustion (69.19%) are much higher than that of TFF (36.86%). This demonstrates that the TPF foam, due to the flame-retardant efficiency of PA, provides effective protection for the foam material during the combustion process.

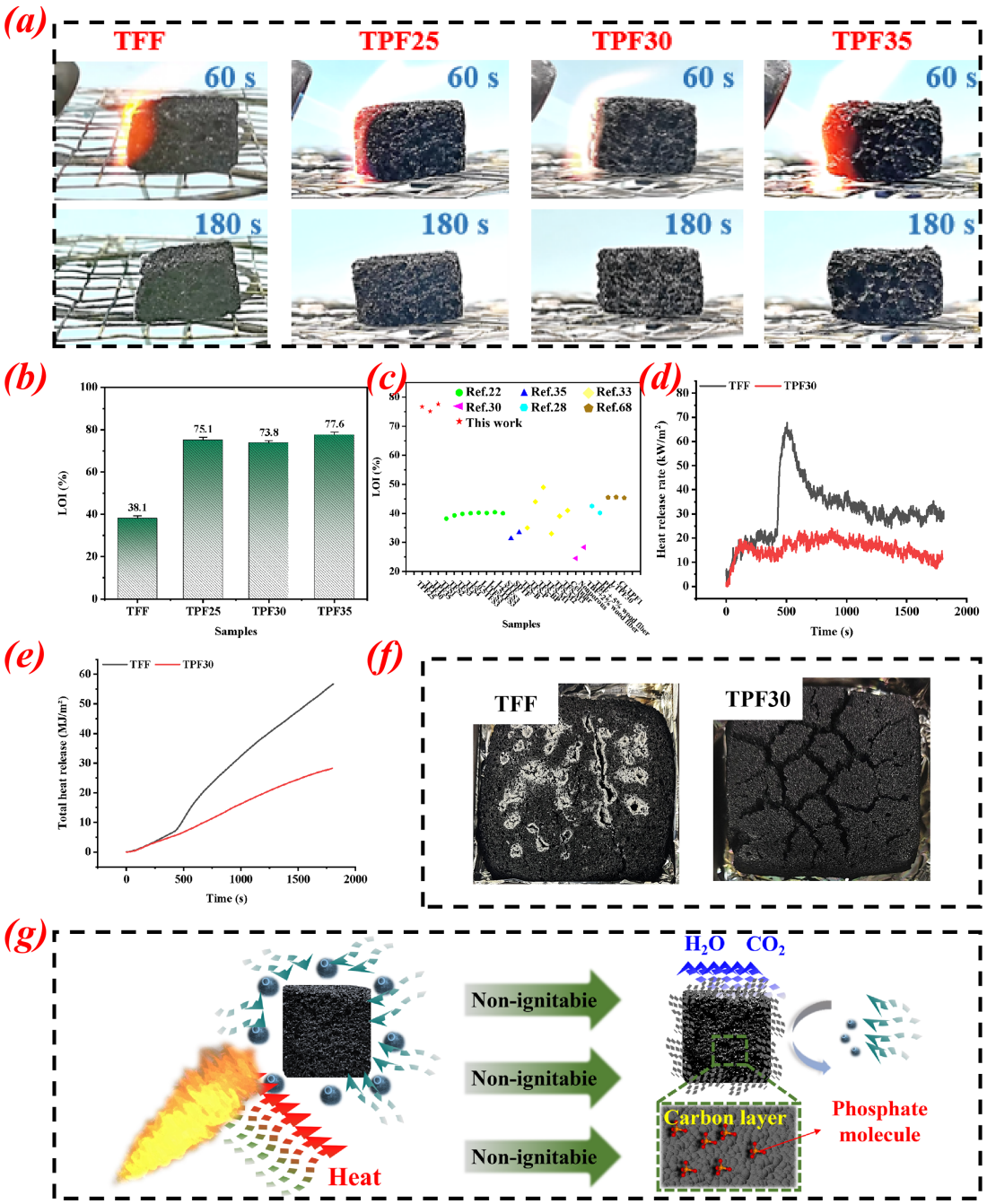

Figure 5: Ignition test of foams (**a**), limiting oxygen index of foams (**b**), comparison of LOI with other literature materials (**c**), heat release rate curves (**d**), total heat release curves (**e**), morphology of foam samples after combustion (**f**), and a plausible flame-retardant mechanism (**g**) of the adapted Tannin-furanic-PA foam.

Table 5: Partial cone calorimetry test data for the different foams.

Samples	TTI (s)	pHRR (kW/m^2)	THR (MJ/m^2)	pSPR (m^2/s)	TSR (m^2)	Residue (wt%)
TFF	456	67.81	56.72	0.0041	0.18	36.86
TPF30	–	24.09	28.31	0.0024	0.37	69.19

Note: TTI, pHRR, THR, pSPR, TSR, and residue represent the ignition time, peak heat release rate, total heat release, peak smoke production rate, total smoke production, and residual amount after tests, respectively.

Fig. 5g illustrates the flame-retardant mechanism of TPF30. Upon heating, the high-phosphorus-content PA decomposes and releases phosphoric acid molecules, accelerating matrix carbonization and insulating or slowing down heat transfer and material exchange between the polymer and the external environment [47,48]. Additionally, the high-carbon-content polyphenol structure leads to increased char yield at elevated temperatures, thereby providing a stronger thermal barrier for the foam, further blocking contact between the combustion interface and air, and better protecting the foam material. In the condensed phase, decomposition of PA generates strong dehydrating species such as phosphoric acid, metaphosphoric acid and polyphosphoric acid. These substances rapidly condense with the hydroxyl groups in the system, forming a dense, continuous and heat-resistant phosphorus-containing carbon layer on the foam surface [49,50]. Unlike traditional dense materials, the open/closed cell composite structure of the TPF30 foam itself plays a physical barrier role in the early stage of combustion. The uniformly distributed pores of TPF30 restrict the diffusion of oxygen into the material interior, while providing abundant reaction sites for the carbonization reaction. Furthermore, in the gas phase, PA decomposes to generate phosphorus-containing free radicals. These radicals capture the highly active free radicals produced during the propagation reaction of polymer combustion, thereby interrupting the chain propagation process. At the same time, TPF30 releases non-flammable gases, including water steam and carbon dioxide during thermal degradation; these gases make the oxygen concentration around TPF30 and the concentration of combustible components in the boundary layer diluted, further suppressing the flame spread to a certain extent [51].

3.6 Application Prospects of Foams

In this work, the thermal conductivity of the PA-adapted tannin-furanic foam is 0.0404–0.0460 W/(m·K), which has the potential for application in building insulation and heat preservation materials [52]. PA enhanced the mechanical strength of the tannin-furanic foam material and, to a certain extent, reduced the corrosive effect on the substrate caused by acid leaching. This enhances its usability in the field of building insulation. As shown in Fig. 6a, when TPF foam material is applied to the exterior walls of buildings, it can replace traditional polyurethane insulation materials and reduce the heat transfer between the interior and exterior of buildings. The key point is that the high flame retardancy of TPF can also provide certain guarantees for the fire safety of buildings, ensuring safety during construction and living. Furthermore, TPF also has certain application potential in packaging materials. Compared with traditional polyurethane (PU) foams and polystyrene (PS) foams, TPF has the advantage of being environmentally friendly. The strength enhancement of TPF catalyzed by PA provides a higher foundation guarantee during application. More importantly, the lower thermal conductivity of TPF offers thermal insulation capabilities for application as packaging materials (Fig. 6b). The PA-modified tannin-furan foam (TPF) possesses excellent thermal insulation and fire resistance properties, as well as environmental friendliness and recyclability. It has shown great potential for application in both building insulation and as packaging materials.

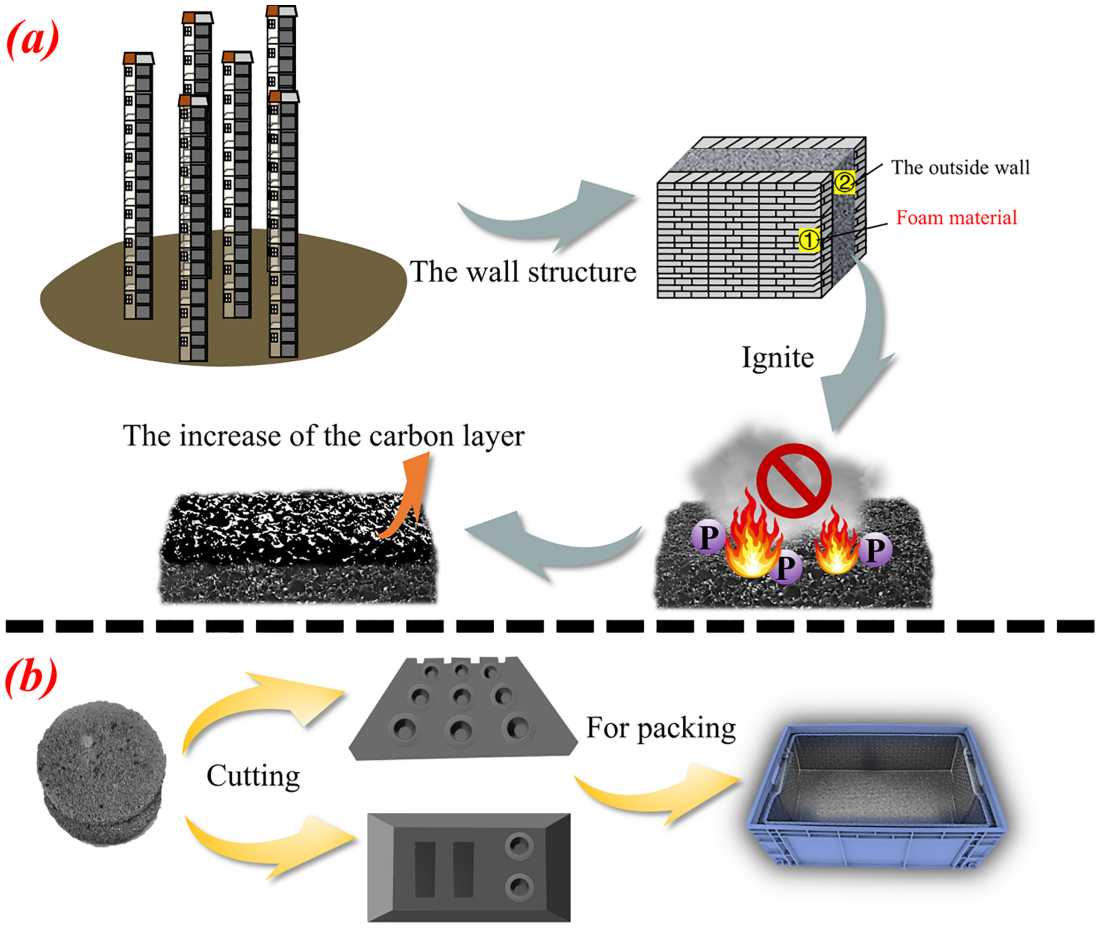

Figure 6: Application potential of foam in construction (**a**) and packaging (**b**).

4 Conclusion

In this study, PA completely replaced *p*-TSA to prepare PA-catalyzed tannin-furanic foams (TPF). Laboratory tests on TPF showed that PA is covalently anchored into the foam network, achieving a higher retention ratio than that of *p*-TSA, thereby effectively suppressing acid leaching. Moreover, the obtained TPF foam exhibited excellent compressive strength, which is more than 34% higher than that of conventional foam, while its thermal conductivity was low, meeting the requirements for building insulation. Compared with traditional tannin-furanic foams, TPF possesses superior flame retardancy, self-extinguishing behavior, and reduced environmental impact. Therefore, PA served a double function as a catalyst and a flame retardant, avoiding the compatibility and mechanical property deterioration often caused by the addition of external flame retardants, and offered new insights for the design of acid-catalyzed systems in biomass-based foaming materials.

Acknowledgement: We thank all the authors for their contributions to this work.

Funding Statement: This research was funded by the National Key R&D Program of China (2023YFD2202100). This work was also supported by the "Xingdian Talents Support Plan" Yunling Scholar and Youth Talent programs, the 111 project (D21027), National High-end Foreign Expert Project (Grant No. H20250253), Yunnan Provincial Expert Workstation (202305AF150006), Yunnan Foreign Experts Project (202505A0120006) and the Joint Special Project on Agricultural Basic Research of Yunnan Province (Grant No. 202301BD070001-25).

Author Contributions: Wenhe Bi: Writing—review & editing, Writing—original draft, Software, Methodology, Investigation. Yang Yang: Writing—review & editing, Validation. Jiamin Wu: Software, Validation. Jianji Chu: Validation. Jun Zhang: Validation. Guanben Du: Writing—review & editing, Resources, Project administration, Data curation. Hisham Essawy: Writing—review & editing, Validation, Methodology. Bertrand Charrier: Writing—review & editing, Validation. Antonio Pizzi: Writing—review & editing, Validation. Xinyi Chen: Writing—review & editing, Validation, Supervision, Project administration, Funding acquisition, Conceptualization. Mingzhi Zhu: Visualization, Validation, Methodology, Formal analysis. Xiaojian Zhou: Writing—review & editing, Writing—original draft, Supervision, Funding acquisition. All authors reviewed and approved the final version of the manuscript.

Availability of Data and Materials: Data will be made available on request.

Ethics Approval: Not Applicable.

Conflicts of Interest: The authors declare no conflicts of interest.

References

1. Meikleham NE, Pizzi A. Acid- and alkali-catalyzed tannin-based rigid foams. J Appl Polym Sci. 1994; 53(11):1547–56. doi:10.1002/app.1994.070531117.
2. Zhu G, Wang J, Yuan X, Yuan B. Hydrophobic and fire safe polyurethane foam coated with chitosan and nano-montmorillonite via layer-by-layer assembly for emergency absorption of oil spill. Mater Lett. 2022;316:132009. doi:10.1016/j.matlet.2022.132009.
3. Razali NIM, Ali F, Azmi AS, Ismail TNMT, Mirghani MES, Omar MF. Microwave-assisted synthesis of polylactic acid-diol for polyurethane as biodegradable packaging material. IOP Conf Ser Mater Sci Eng. 2021;1192(1):012015. doi:10.1088/1757-899X/1192/1/012015.
4. Amirabadi S, Ramezani Kakroodi A, Dias OAT, Sain M, Park CB. Tailoring nano-fibrillated polystyrene composite with enhanced fire retarding properties for foam applications. Mater Des. 2022;214(1):110419. doi:10.1016/j.matdes.2022.110419.
5. Liu C, Xie Y, Gao D, Shi X, Rao Z. Fabrication of fire-retardant building materials via a hyper-crosslinking chemical conversion process from waste polystyrenes. Energy Built Environ. 2022;3(2):226–32. doi:10.1016/j.enbenv.2021.01.008.
6. Sarika PR, Nancarrow P, Makkawi Y, Ibrahim TH. Preparation and characterization of date palm bio-oil modified phenolic foam. Polymers. 2024;16(7):955. doi:10.3390/polym16070955.
7. Kumar D, Alam M, Zou PXW, Sanjayan JG, Memon RA. Comparative analysis of building insulation material properties and performance. Renew Sustain Energy Rev. 2020;131(7):110038. doi:10.1016/j.rser.2020.110038.
8. Azlina Ramlee N, Jawaid M, Abdul Karim Yamani S, Syams Zainudin E, Alamery S. Effect of surface treatment on mechanical, physical and morphological properties of oil palm/bagasse fiber reinforced phenolic hybrid composites for wall thermal insulation application. Constr Build Mater. 2021;276(174):122239. doi:10.1016/j.conbuildmat.2020.122239.
9. Basso MC, Giovando S, Pizzi A, Celzard A, Fierro V. Tannin/furanic foams without blowing agents and formaldehyde. Ind Crops Prod. 2013;49(12):17–22. doi:10.1016/j.indcrop.2013.04.043.
10. Chen X, Li J, Pizzi A, Fredon E, Gerardin C, Zhou X, et al. Tannin-furanic foams modified by soybean protein isolate (SPI) and industrial lignin substituting formaldehyde addition. Ind Crops Prod. 2021;168:113607. doi:10.1016/j.indcrop.2021.113607.
11. Xu C, Sun C, Wan H, Tan H, Zhao J, Zhang Y. Microstructure and physical properties of poly(lactic acid)/polycaprolactone/rice straw lightweight bio-composite foams for wall insulation. Constr Build Mater. 2022;354(8):129216. doi:10.1016/j.conbuildmat.2022.129216.
12. Varila T, Romar H, Luukkonen T, Hilli T, Lassi U. Characterization of lignin enforced tannin/furanic foams. Heliyon. 2020;6(1):e03228. doi:10.1016/j.heliyon.2020.e03228.
13. Li X, Basso MC, Fierro V, Pizzi A, Celzard A. Chemical modification of tannin/furanic rigid foams by isocyanates and polyurethanes. Maderas-Cienc Tecnol. 2014;14(3):257–66. doi:10.4067/s0718-221x2012005000001.

14. Zhou X, Pizzi A, Sauget A, Nicollin A, Li X, Celzard A, et al. Lightweight tannin foam/composites sandwich panels and the coldset tannin adhesive to assemble them. Ind Crops Prod. 2013;43:255–60. doi:10.1016/j.indcrop.2012.07.020.
15. Li J, Liao J, Essawy H, Zhang J, Li T, Wu Z, et al. Preparation and characterization of novel cellular/nonporous foam structures derived from tannin furanic resin. Ind Crops Prod. 2021;162(1):113264. doi:10.1016/j.indcrop.2021.113264.
16. Pizzi A. Tannin-based biofoams-a review. J Renew Mater. 2019;7(5):477–92. doi:10.32604/jrm.2019.06511.
17. Sim GY, Lee SU, Lee JW. Enhanced extraction of phytic acid from rice hulls with enzymatic treatment and production of ethanol from reducing sugars in hydrolyzed rice hulls after extraction of phytic acid. LWT. 2020;133:110111. doi:10.1016/j.lwt.2020.110111.
18. Gao S, Wang J, Wang K, Cai Y, Li C, Dong Y, et al. Efficient solar-driven interfacial desalination of wood through surface furfurylation. Colloids Surf A Physicochem Eng Aspects. 2025;709:136161. doi:10.1016/j.colsurfa.2025.136161.
19. He S, Gao YY, Zhao ZY, Huang SC, Chen ZX, Deng C, et al. Fully bio-based phytic acid–basic amino acid salt for flame-retardant polypropylene. ACS Appl Polym Mater. 2021;3(3):1488–98. doi:10.1021/acsapm.0c01356.
20. Zhao X, Liu T, Ou R, Hao X, Fan Q, Guo C, et al. Fully biobased soy protein adhesives with integrated high-strength, waterproof, mildew-resistant, and flame-retardant properties. ACS Sustain Chem Eng. 2022;10(20):6675–86. doi:10.1021/acssuschemeng.2c00742.s001.
21. Oo CW, Kassim MJ, Pizzi A. Characterization and performance of *Rhizophora apiculata* mangrove polyflavonoid tannins in the adsorption of copper (II) and lead (II). Ind Crops Prod. 2009;30(1):152–61. doi:10.1016/j.indcrop.2009.03.002.
22. Ricci A, Olejar KJ, Parpinello GP, Kilmartin PA, Versari A. Application of Fourier transform infrared (FTIR) spectroscopy in the characterization of tannins. Appl Spectrosc Rev. 2015;50(5):407–42. doi:10.1080/05704928.2014.1000461.
23. Dong J, Wen Y, Miao Y, Xie Z, Zhang Z, Yang H. A nanoporous zirconium phytate film for immobilization of redox protein and the direct electrochemical biosensor. Sens Actuat B Chem. 2010;150(1):141–7. doi:10.1016/j.snb.2010.07.029.
24. Tarafdar A, Panda AB, Pradhan NC, Pramanik P. Synthesis of spherical mesostructured zirconium phosphate with acidic properties. Microporous Mesoporous Mater. 2006;95(1–3):360–5. doi:10.1016/j.micromeso.2006.05.008.
25. Zhou M, Liu J, Lu P, Huang Y, Xiao Y, Zhang J, et al. Polyfunctional phytic acid-based reactive diluent for UV-curable coating with improved flame-retardant performance and toughness. Ind Crops Prod. 2023;204:117368. doi:10.1016/j.indcrop.2023.117368.
26. Chen X, Li J, Xi X, Pizzi A, Zhou X, Fredon E, et al. Condensed tannin-glucose-based NIPU bio-foams of improved fire retardancy. Polym Degrad Stab. 2020;175(7):109121. doi:10.1016/j.polymdegradstab.2020.109121.
27. Rao WH, Zhu ZM, Wang SX, Wang T, Tan Y, Liao W, et al. A reactive phosphorus-containing polyol incorporated into flexible polyurethane foam: self-extinguishing behavior and mechanism. Polym Degrad Stab. 2018;153:192–200. doi:10.1016/j.polymdegradstab.2018.04.029.
28. Chen X, Pizzi A, Fredon E, Gerardin C, Zhou X, Zhang B, et al. Low curing temperature tannin-based non-isocyanate polyurethane (NIPU) wood adhesives: preparation and properties evaluation. Int J Adhes Adhes. 2022;112:103001. doi:10.1016/j.ijadhadh.2021.103001.
29. Tondi G, Cefarin N, Sepperer T, D'Amico F, Berger RJF, Musso M, et al. Understanding the polymerization of polyfurfuryl alcohol: ring opening and Diels-alder reactions. Polymers. 2019;11(12):2126. doi:10.3390/polym11122126.
30. Zhou F, Zhang T, Zou B, Hu W, Wang B, Zhan J, et al. Synthesis of a novel liquid phosphorus-containing flame retardant for flexible polyurethane foam: combustion behaviors and thermal properties. Polym Degrad Stab. 2020;171(3):109029. doi:10.1016/j.polymdegradstab.2019.109029.
31. Celzard A, Zhao W, Pizzi A, Fierro V. Mechanical properties of tannin-based rigid foams undergoing compression. Mater Sci Eng A. 2010;527(16–17):4438–46. doi:10.1016/j.msea.2010.03.091.
32. Tondi G, Oo CW, Pizzi A, Trosa A, Thevenon MF. Metal adsorption of tannin based rigid foams. Ind Crops Prod. 2009;29(2–3):336–40. doi:10.1016/j.indcrop.2008.06.006.

33. Wu X, Yan W, Zhou Y, Luo L, Yu X, Luo L, et al. Thermal, morphological, and mechanical characteristics of sustainable tannin bio-based foams reinforced with wood cellulosic fibers. Ind Crops Prod. 2020;158(67):113029. doi:10.1016/j.indcrop.2020.113029.
34. Gao C, Li M, Zhu C, Hu Y, Shen T, Li M, et al. One-pot depolymerization, demethylation and phenolation of lignin catalyzed by HBr under microwave irradiation for phenolic foam preparation. Compos Part B Eng. 2021;205(6414):108530. doi:10.1016/j.compositesb.2020.108530.
35. Zhao J, Yang X, Yang Y, Liu L, Lin Y, Xie L, et al. Biomass polyamine-functionalized nanocellulose-loaded covalent organic framework to construct composite aerogels for highly efficient removal of Cr (VI) and methyl orange. Chem Eng J. 2024;486:150282. doi:10.1016/j.cej.2024.150282.
36. Yin K, Liu M, Shao Z, Chen C, Wu W, Tan Y, et al. Enhancing flame retardancy and smoke suppression of lignocellulose through modification with green aqueous flame retardants. Ind Crops Prod. 2025;225:120493. doi:10.1016/j.indcrop.2025.120493.
37. Liu Z, Lin X, Mai X, Zhuang J, Guo F, Yang R, et al. Ambient drying fabrication of mechanically robust, flame-retardant, thermal-insulating cellulose/aramid nanofiber composite foam via freeze-casting combined ion cross-linking. Carbohydr Polym. 2025;353:123269. doi:10.1016/j.carbpol.2025.123269.
38. Sun WB, Han ZM, Luo XH, Yang HB, Liu ZX, Li DH, et al. Strong and fireproof regenerated wood via a combined phosphorylation-surface nanofibrillation and ionic cross-linking strategy. ACS Nano. 2025;19(3):3602–13. doi:10.1021/acsnano.4c13857.s002.
39. Zhang A, Li J, Zhang S, Mu Y, Zhang W, Li J. Characterization and acid-catalysed depolymerization of condensed tannins derived from larch bark. RSC Adv. 2017;7(56):35135–46. doi:10.1039/c7ra03410e.
40. Li J, Zhang A, Zhang S, Gao Q, Zhang W, Li J. Larch tannin-based rigid phenolic foam with high compressive strength, low friability, and low thermal conductivity reinforced by cork powder. Compos Part B Eng. 2019;156(6):368–77. doi:10.1016/j.compositesb.2018.09.005.
41. Li X, Liu B, Zheng L, Essawy H, Liu Z, Liu C, et al. Facile synthesis of formaldehyde-free bio-based thermoset resins for fabrication of highly efficient foams. Polymers. 2022;14(23):5140. doi:10.3390/polym14235140.
42. Yuan W, Xi X, Zhang J, Pizzi A, Essawy H, Du G, et al. A novel strategy inspired by steaming Chinese steamed bread for preparation of tannin-furanic rigid bio-foam. Constr Build Mater. 2023;376(1):131035. doi:10.1016/j.conbuildmat.2023.131035.
43. Kong L, Guan H, Wang X. *In situ* polymerization of furfuryl alcohol with ammonium dihydrogen phosphate in poplar wood for improved dimensional stability and flame retardancy. ACS Sustain Chem Eng. 2018;6(3):3349–57. doi:10.1021/acssuschemeng.7b03518.
44. Cao ZJ, Liao W, Wang SX, Zhao HB, Wang YZ. Polyurethane foams with functionalized graphene towards high fire-resistance, low smoke release, superior thermal insulation. Chem Eng J. 2019;361:1245–54. doi:10.1016/j.cej.2018.12.176.
45. Li W, Zhang A, Luo F, Dai Y, Chen D, Chen Q, et al. Excellent flame retardant of flexible polyurethane foams with green coatings by sol–gel method. J Appl Polym Sci. 2025;142(32):e57277. doi:10.1002/app.57277.
46. Bellayer S, Jimenez M, Barrau S, Bourbigot S. Fire retardant sol–gel coatings for flexible polyurethane foams. RSC Adv. 2016;6(34):28543–54. doi:10.1039/c6ra02094a.
47. Zhu G, Huang Y, Wang Z, Zhu Z, Xiao F. N/P/S synergistic design of epoxy composites towards flame retardancy, Acid/Alkali resistance and comprehensive performance. Polym Degrad Stab. 2026;247(2):111983. doi:10.1016/j.polymdegradstab.2026.111983.
48. Zhu Z, Gao J, Zhu G, Huang Y, Wang Z, Feng J, et al. APP and MXene collision: multiscale interface engineering-driven fire-retardant polylactide with mechanical toughness. Compos Part B Eng. 2026;312(7633):113344. doi:10.1016/j.compositesb.2025.113344.
49. Liu Y, Zhang A, Cheng Y, Li M, Cui Y, Li Z. Recent advances in biomass phytic acid flame retardants. Polym Test. 2023;124(8):108100. doi:10.1016/j.polymertesting.2023.108100.
50. Naiker VE, Mestry S, Nirgude T, Gadgeel A, Mhaske ST. Recent developments in phosphorous-containing bio-based flame-retardant (FR) materials for coatings: an attentive review. J Coat Technol Res. 2023;20(1):113–39. doi:10.1007/s11998-022-00685-z.

51. Li M, Huang Y, Yang L, Li L, Xu J. A novel flame retardant epoxy thermoset based on renewable honokiol and furfuryl alcohol. Constr Build Mater. 2024;432(3):136707. doi:10.1016/j.conbuildmat.2024.136707.
52. Abu-Jdayil B, Mourad AH, Hittini W, Hassan M, Hameedi S. Traditional, state-of-the-art and renewable thermal building insulation materials: an overview. Constr Build Mater. 2019;214(3):709–35. doi:10.1016/j.conbuildmat.2019.04.102.